EMPIRICAL CORRECTION OF RHESSI SPECTRA FOR PHOTOSPHERIC ALBEDO AND ITS EFFECT ON INFERRED ELECTRON SPECTRA

R. CALUM ALEXANDER and JOHN C. BROWN
Department of Physics and Astronomy, University of Glasgow, Glasgow G12 8QQ, U.K.

(Received 6 August 2002; accepted 22 August 2002)

Abstract. Photospheric Compton backscatter (albedo) makes a significant contribution to observed hard X-ray (HXR) spectral fluxes over the RHESSI energy range and should be allowed for in HXR spectral interpretation. The full correction problem is nonlinear and messy but we offer a simple approximate first-order correction procedure for global HXR spectra based upon empirical fits to published albedo simulations. We also illustrate the impact of this correction on inferred electron spectra for the thin- and thick-target models.

1. Introduction

The high HXR spectral resolution of RHESSI creates the chance for precise study of source electron spectra provided the observed spectra are well corrected for non-primary effects at the Sun including albedo, directivity, source ionisation variations and the like. General treatment of all of these is theoretically complex and computationally intensive for each source model one wants to try. Although this should be an eventual goal, for the present it is more useful to have simpler but more versatile methods for first-order correction of spectral data (after optimal removal of the already complex instrumental effects). In this paper we offer such an approach for correction of the photospheric albedo.

It was first pointed out by Tomblin (1972) and by Santangelo, Horstman, and Horstman-Moretti (1973) that some of the primary photons emitted downward around the deka-keV range in the optically thin solar atmosphere undergo Compton backscatter in the low atmosphere and add to the primary photons, emitted upwards, in the observed signal. These albedo photons come from an extended area and arrive with a spread of delay times, depending on the primary source height. It has been suggested that careful imaging (Brown, van Beek, and McClymont, 1975) or time delay (Bai, 1978) studies could help infer source heights. In this paper we restrict ourselves solely to considering the effect of the albedo contribution on the spectrum of the HXR source as a whole.

The spectral distribution of the albedo contribution was studied in detail by Bai and Ramaty (1978) via Compton scattering simulation allowing for photon absorption, and we base our empirical approach (Section 2) on their results. The

Solar Physics **210:** 407–418, 2002.

main need for empirical simplification is the fact that albedo correction is not just a spectral correction factor (like a 'coloured' mirror) but strictly speaking is itself a convolution. That is, the fractional albedo addition A(ϵ) at photon energy ϵ to the primary photon spectrum $I_0(\epsilon)$ itself depends on the functional form of $I_0(\epsilon)$, since Compton scattering shifts photons in energy. Thus recovery of $I_0(\epsilon)$ from the total observed spectrum $I(\epsilon)$ involves inversion of a nonlinear convolution of $I_0(\epsilon)$ with the scattering and absorption processes.

2. Empirical Albedo Correction to Spectra

Suppose the total primary HXR source emission rate is $I_0(\epsilon)$ (photons cm^{-2} s^{-1} per unit ϵ) as seen at the Earth. The actual total rate $I(\epsilon)$ as seen from the Sun can be written as

$$I_{\text{tot}}(\epsilon) = I_0(\epsilon)(1 + A_{I_0}(\epsilon)), \tag{1}$$

where $A_{I_0}(\epsilon)$ is the fractional albedo contribution at energy ϵ. This depends, as mentioned, on $I_0(\epsilon)$ itself as well as on ϵ explicitly. In fact A_{I_0} also depends somewhat on the source geometry; specifically on the source height above the photosphere and the heliocentric-angle of the source, since Compton backscatter is angle and energy dependent. Since variation across the disk is not large and is more of a scale factor than a spectral distortion, here we ignore it and use angle-averaged results from Bai and Ramaty (1978), though our approach could readily by extended to apply to each flare heliocentric angle separately by fitting of our empirical form to the appropriate Bai and Ramaty results for that angle.

Bai and Ramaty computed $A_{I_0}(\epsilon)$ for the specific forward problem of a simple power-law $I_0(\epsilon) \sim \epsilon^{-\gamma}$ and for these cases we can write

$$A_{I_0}(\epsilon) = A_\gamma(\epsilon). \tag{2}$$

What we would like is a simplified procedure to estimate $I_0(\epsilon)$ from $I(\epsilon)$ allowing for the influence of $A(\epsilon)$ and we propose the following:

(1) Since A, while significant, is never large or rapidly varying, obtain a first approximation to $I_0(\epsilon)$ as a power law $\sim \epsilon^{-\gamma}$ by best fitting the total data $I(\epsilon)$ to a power-law index γ. (Essentially taking $A =$ constant to zeroth order).

(2) Use the best fit γ from step (1) with the Bai and Ramaty results on $A_\gamma(\epsilon)$ for a power law $I_0(\epsilon)$ to obtain a first-order estimate of $A_{I_0}(\epsilon)$ using Equation (2).

(3) Adopt this $A_\gamma(\epsilon)$ in Equation (1) to derive a first-order albedo-corrected $I_0(\epsilon) = I_{\text{tot}}(\epsilon)/(1 + A_\gamma(\epsilon))$.

To make this easy to do in practice we have explored convenient parameterized forms of $A_\gamma(\epsilon)$ and best fit the (γ dependent) parameters to the Bai and Ramaty results for each of the four different γ values which they simulated. We found a convenient form was

TABLE I
Best-fit parameters to the Bai and Ramaty data.

γ	A_0	a	b
2	0.0077	1.53	0.31
3	0.0088	1.46	0.34
4	0.0098	1.41	0.37
5	0.0111	1.34	0.38

$$A_\gamma(\epsilon) = A_0(\gamma)\left(\frac{\epsilon}{10}\right)^{a(\gamma)} e^{-b(\gamma)(\epsilon/10)}, \tag{3}$$

where ϵ is in keV and the best fit values for of A_0, a, and b are given in Table I. In Figures 1(a–d) we show the Bai and Ramaty $A_\gamma(\epsilon)$ results with our best fit superimposed.

Figures 1(a–d) show the plots of the best-fit parameters given in Table I for $A_0(\gamma)$, $a(\gamma)$, and $b(\gamma)$ substituted into (3) (full line) compared with the Bai and Ramaty data (symbols) for the four values of γ studied.

Bai and Ramaty only computed four cases of γ. To extend these fits empirically to general γ we show in Figures 2(a–c) plots of $A_0(\gamma)$, $a(\gamma)$, and $b(\gamma)$ versus γ with linear fits through these four points.

Figures 2(a–c) show the plots of the best-fit parameters given in Table I for $A_0(\gamma)$, $a(\gamma)$, and $b(\gamma)$. A linear fit straight line through the data points is shown for each parameter.

3. Effect of Albedo Correction on Inferred Electron Spectra

3.1. Formulation

Given $I_0(\epsilon)$, one can derive the source mean electron spectrum $\bar{F}(E)$ ('thin-target') and the collisional thick-target electron injection spectrum $\mathcal{F}_0(E_0)$ by inversion of the bremstrahlung spectral integral. This was shown analytically by Brown (1971) for the Bethe–Heitler cross section and by Brown and Emslie (1988) for the Kramer's cross-section. Here we use the Kramer's analytic case to demonstrate how large the effect of $A(\epsilon)$ can be on inference of source electron spectra. Specifically we: (a) consider cases where the primary electron spectra are in fact power law ($E^{-\delta}$ or $E_0^{-\delta}$), resulting in power law $I_0(\epsilon)$ in both cases (with $\gamma = \delta+1, \delta-1$, respectively), (b) generate the total $I_{\rm tot}(\epsilon) = I_0(\epsilon)(1 + A(\epsilon))$ that would be observed using Equation (3), (c) use the analytic inversion formulae to find out what

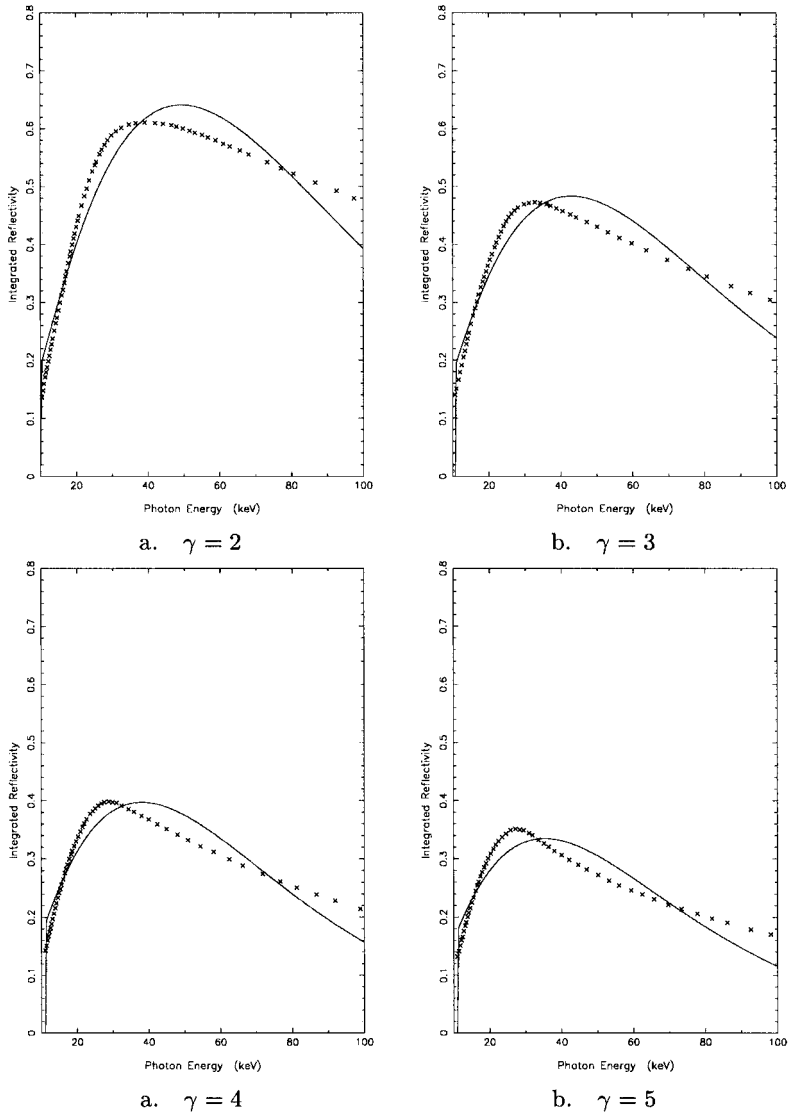

Figure 1. Plots of best-fit parameters (*solid line*), along with the Bai and Ramaty data for the 10–100 keV photon energy range.

$\bar{F}(E)$, $\mathcal{F}_0(E_0)$ would be derived from that $I_{\text{tot}}(\epsilon)$ if albedo were ignored, i.e., if it were assumed that $I_0 = I_{\text{tot}}$.

The *normalized* Kramer's approximation to the bremstrahlung cross-section is

$$Q(\epsilon, E) = \frac{Q_0}{\epsilon E} q(\epsilon, E),$$

where $q = 1$ and Q_0 is a constant.

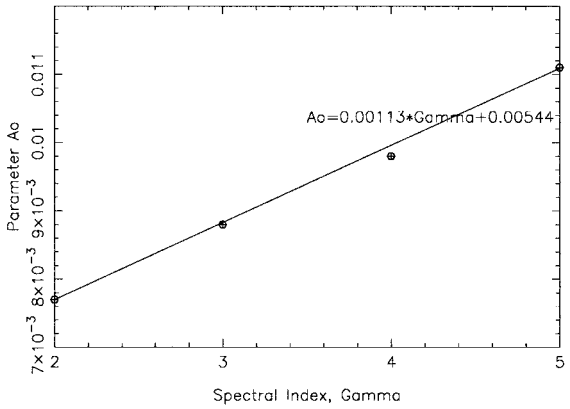

a. Linear fit for parameter A_o

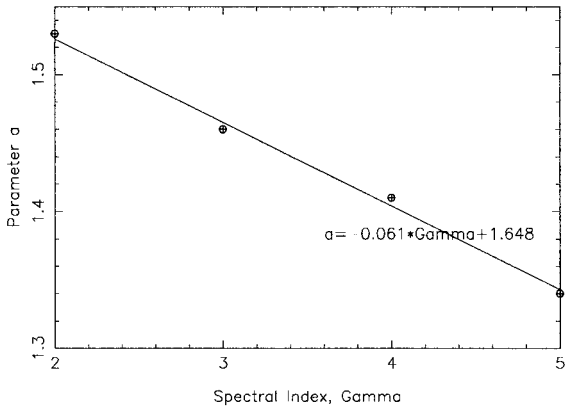

b. Linear fit for parameter a

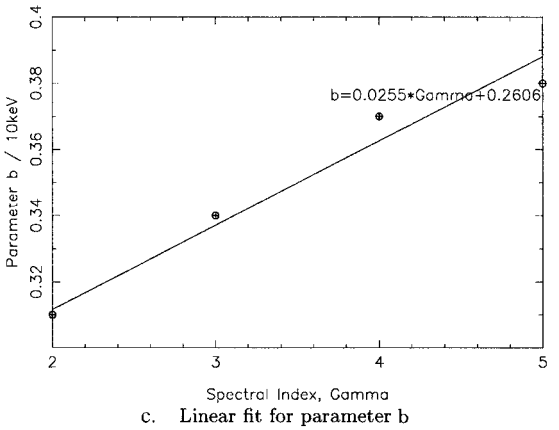

c. Linear fit for parameter b

Figure 2. Plots of linear fits through the best-fit parameters $A_0(\gamma)$, $a(\gamma)$, and $b(\gamma)$.

3.2. THIN TARGET

For this case the solution for the mean (thin-target) electron spectrum $\bar{F}(E)$ in a source of mean density $\bar{n}_p$, volume V is (Brown and Emslie, 1988)

$$\bar{F}(E) = \frac{1}{\bar{n}_p V Q_0} E \left[-\frac{\mathrm{d}}{\mathrm{d}\epsilon}(\epsilon I(\epsilon)) \right]_{\epsilon=E}. \tag{4}$$

In the case of a power law

$$I_0(\epsilon) = C\epsilon^{-\gamma}, \tag{5}$$

this yields

$$\bar{F}(E) \equiv \bar{F}_0(E) = \frac{(\gamma-1)C}{\bar{n}_p V Q_0} E^{-\gamma+1}. \tag{6}$$

However, in reality we observe $I_{\mathrm{tot}} = I_0(1 + A(\epsilon))$ rather than I_0 and if we ignore the albedo correction by misidentifying I_{tot} (Equations (3) and (5)) with I_0 then by (4) – we would infer

$$\bar{F}(E) = \frac{(\gamma-1)C}{\bar{n}_p V Q_0} E^{-\gamma+1} \left[1 - A_0 E^a e^{-bE} \frac{(1 + a - (\gamma + bE))}{\gamma - 1} \right], \tag{7}$$

which is shown in Figure 3(a–d), or a mean electron spectrum wrong by a fractional error

$$f_{\mathrm{thin}}(\gamma) = \frac{\Delta\bar{F}(E)}{\bar{F}_0(E)} = \frac{\bar{F}(E) - \bar{F}_0(E)}{\bar{F}_0(E)} = \frac{A_0 E^a e^{-bE} \left[(\gamma + bE) - (a+1) \right]}{\gamma - 1}, \tag{8}$$

which is shown in Figure 4.

3.3. THICK TARGET

Here the relevant electron spectrum is the total electron injection rate $\mathcal{F}_0(E_0)$ electrons per s per unit E_0 and is given from the photon spectrum by Brown and Emslie (1988) (with $K = 2\pi e^4 \Lambda$):

$$\mathcal{F}_0(E_0) = \frac{K}{Q_0} \left[\frac{\mathrm{d}^2}{\mathrm{d}\epsilon^2}(\epsilon I_0(\epsilon)) \right]_{\epsilon=E_0}. \tag{9}$$

For a primary power-law $I_0(\epsilon)$, (5), this leads to

$$\mathcal{F}_0(E_0) = \frac{K}{Q_0} C(\gamma - 1) E_0^{-\gamma-1}, \tag{10}$$

while if the albedo correction is added to I_0 and I_{tot} is misinterpreted as I_0 then one obtains

$$\mathcal{F}(E_0) = \frac{K}{Q_0} C E_0^{-\gamma} \times$$
$$\times \left[\frac{\gamma}{E_0}(\gamma - 1) + A_0 \epsilon^a e^{-b\epsilon} \left((\gamma - 1)(\frac{\gamma}{E_0} - 2(\frac{a}{E_0} - b)) + \right. \right. \quad (11)$$
$$\left. \left. + E_0 \left((\frac{a}{E_0} - b)^2 - \frac{a}{E_0^2} \right) \right) \right],$$

which is incorrect by a fractional amount

$$f_{\text{thick}}(\gamma) = \frac{\mathcal{F}(E_0) - \mathcal{F}_0(E_0)}{\mathcal{F}_0(E_0)} = \frac{A_0 \epsilon^a e^{-b\epsilon} E_0}{\gamma(\gamma - 1)} \times$$
$$\times \left[(\gamma - 1)(\frac{\gamma}{E_0} - 2(\frac{a}{E_0} - b)) + E_0 \left((\frac{a}{E_0} - b)^2 - \frac{a}{E_0^2} \right) \right],$$

which is shown in Figure 6.

3.4. Resulting correction for the Kramer's cross section

Figures 3(a–d) show the plots of the recovered thin-target Kramer electron spectrum (solid lines) along with their respective primary electron spectrum (broken lines) for the four values of γ studied. The error in the recovered spectrum can be observed as a 'bump' in the spectrum.

Figure 4 shows the fractional difference decreasing as γ increases. It also shows that the inferred electron flux at 'X' keV will be *greater* by 'Y' percent when the effect of an albedo has been included. This percentage also varies with energy. For example, at 100 keV, an error of approximately 35% is obtained for $\gamma = 2$.

Figures 5(a–d) show the log plots of the recovered thick-target Kramer electron spectrum $\mathcal{F}(E_0)$ (solid lines) along with their respective primary electron spectrum $\mathcal{F}_0(E_0)$ (broken lines) for the four values of γ studied.

Figure 6 shows the fractional difference decreasing as γ increases. As previously mentioned for the thin-target case, there is an energy dependent difference in the inferred electron flux where the effect of an albedo has been included. It is also apparent from Figure 6 that the error in the thick-target is significantly greater than in the thin-target case.

4. Discussion

RHESSI spectra have not been reported as exhibiting evident spectral bulges like those shown in Figures 3(a–d) and 5(a–d). In order to redress this apparent discrepancy the following explanations might be offered:

(1) The primary spectrum $I_0(\epsilon)$ had a dip where $A(\epsilon)$ has a bulge, the two offsetting one another. This seems too much of a coincidence to be plausible.

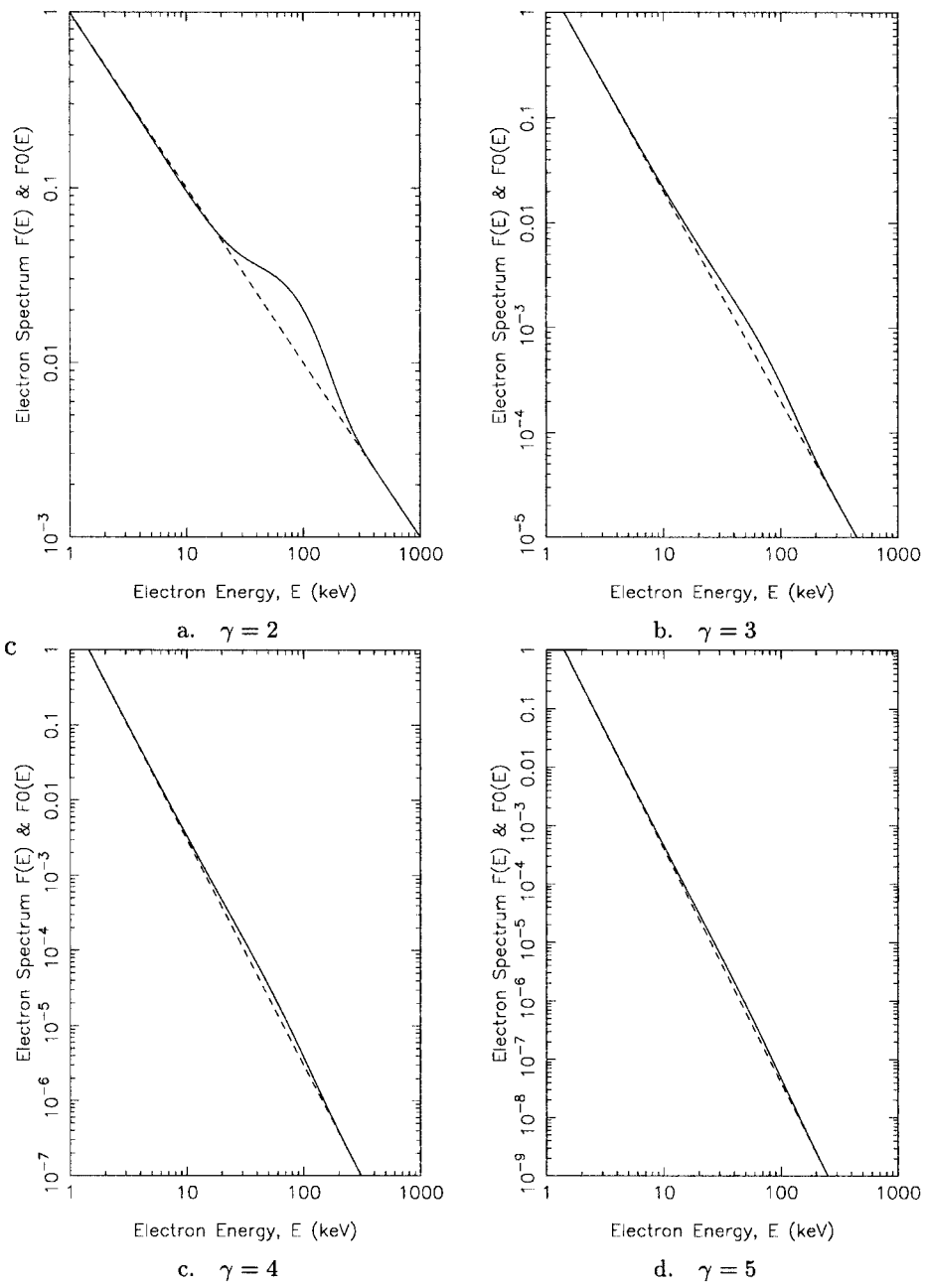

Figure 3. Plots of observed electron spectrum $\bar{F}(E)$ (*solid line*) and primary electron spectrum $\bar{F}_0(E)$ (*dashed line*).

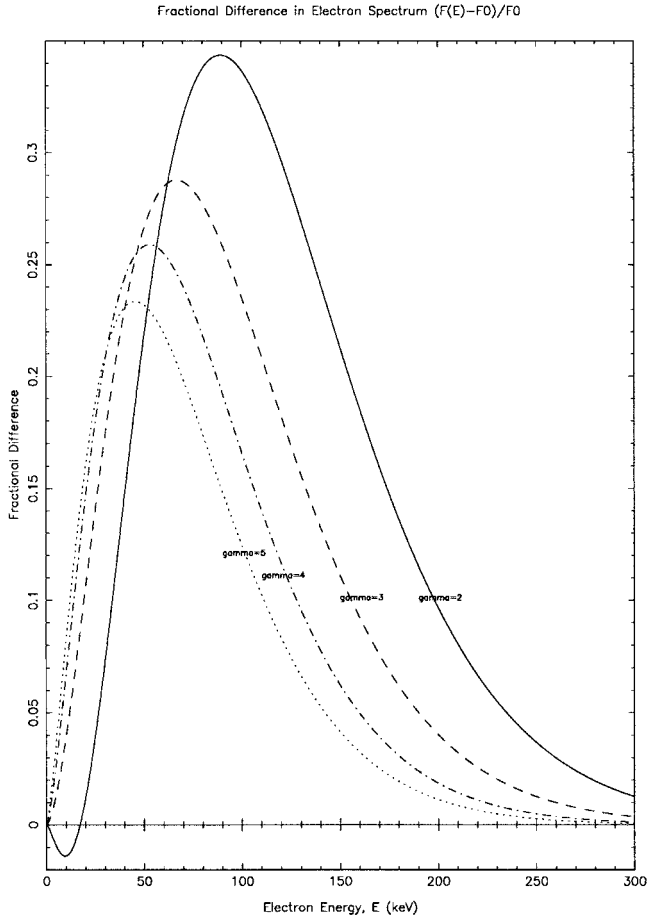

Figure 4. Fractional difference between the observed and primary thin target (Kramer's) electron spectrum showing the fraction difference decreasing with increasing γ.

(2) The bulges are present but have not been specifically noticed or reported as such. In fact, the lower energy end of the bulge is down around 10 keV which may be lost in the thermal emission component. The middle and upper end energy range of the bulge looks somewhat like a downward knee in the deka-keV range. Such features are regularly seen in data, cf., discussion in Kontar, Brown, and McArthur (2002). Albedo may be a partial explanation of these.

(3) There are other corrections – especially that for non-uniform target ionisation in the case of thick-target primary sources discussed by Kontar, Brown, and McArthur (2002) which have been ignored in this paper. Depending on the depth ('energy') of the transition region, this correction might tend to either augment or hide the effect of albedo on the spectrum.

(4) The assumption of an isotropic, point source (Bai and Ramaty, 1978) which provided our source data for $A(\epsilon)$ may require modification.

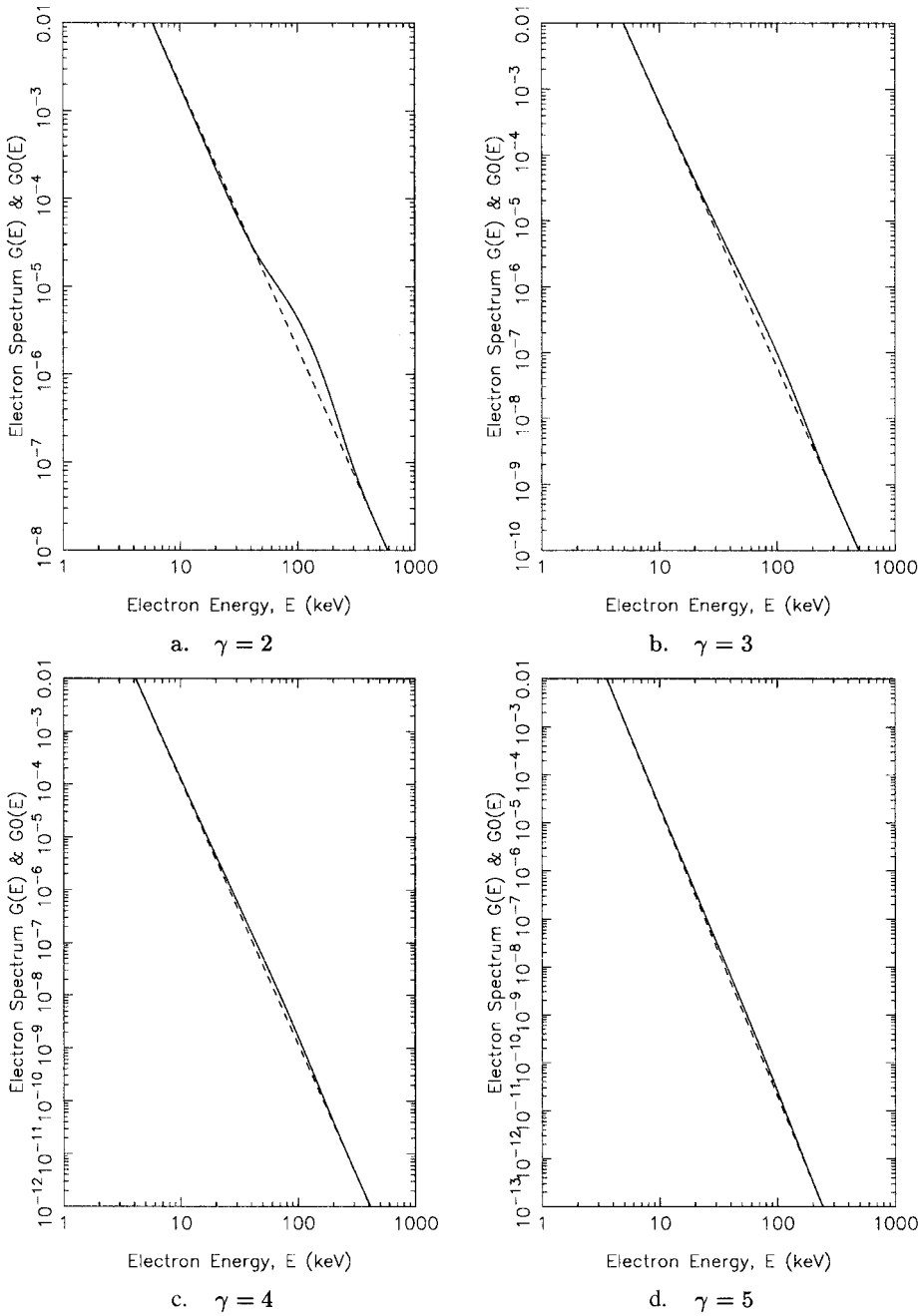

Figure 5. Plots of cold thick-target electron spectrum $\mathcal{F}(E_0)$ (*solid line*) and primary electron spectrum $\mathcal{F}_0(E_0)$ (*dashed line*).

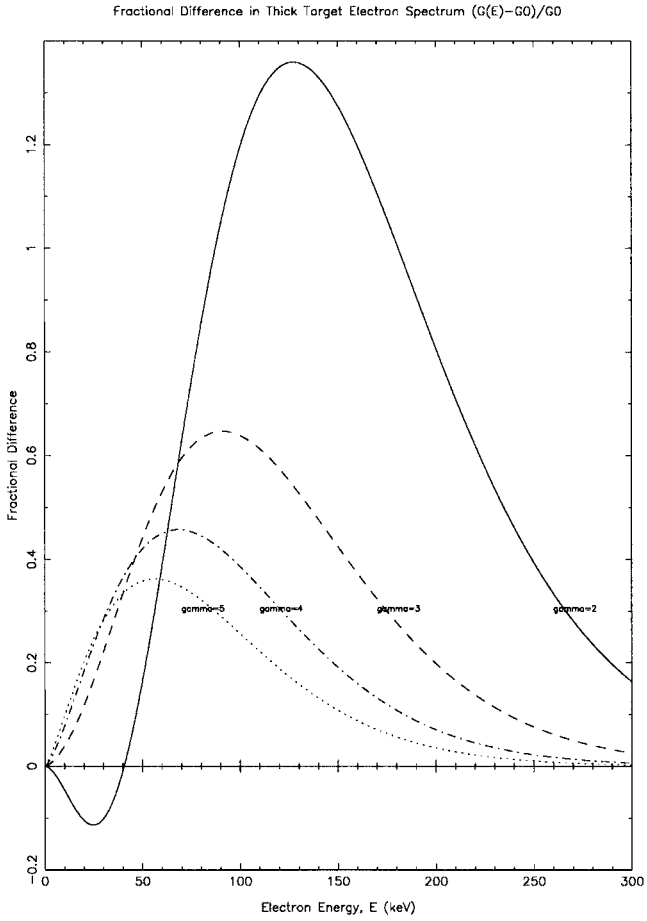

Figure 6. Fractional difference between the observed and primary thick-target electron spectrum.

5. Conclusion

We have explored the effect of photospheric albedo on observations of global flare hard X-ray spectra and derived an expression to allow approximate correction for this in the case of primary power-law photon spectra. We have also examined, for the Kramer's cross-section, the consequences of ignoring the albedo correction in using observed spectra to infer flare source electron spectra for thin and thick target interpretations and shown that the effects are very significant in terms of inferred spectral shape, especially for hard spectra. We have not extended the analysis to other cross sections but we note that the effects of albedo on deriving electron spectra will be even larger for more realistic smoother cross-section approximations, such as the Bethe–Heitler, than for Kramer's because they filter the electron spectral features even more. This is confirmed by our preliminary results for the Bethe–Heitler case, to be presented in a future paper. We also note that the effects

of albedo should be considered alongside other corrections such as that of nonuniform target ionisation in the case of the thick target beam model as discussed by Kontar, Brown and McArthur (2002).

Acknowledgements

This research was in part funded by PPARC. We would also like to acknowledge the input from useful discussions with A. Conway, M. Hendry, and L. Fletcher.

References

Bai, T.: 1978, *Solar Phys.* **59**, 141.
Bai, T. and Ramaty, R.: 1978, *Astrophys. J.* **219**, 705.
Brown, J. C.: 1971, *Solar Phys.* **18**, 489.
Brown, J. C. and Emslie, A. G.: 1988, *Astrophys. J.* **331**, 554.
Brown, J. C., Van Beek, H. F., and McClymont, A. N.: 1975, *Astron. Astrophys.* **41**, 395.
Kontar, E. P., Brown, J. C., and McArthur, G., 2002, *Solar Phys.*, this volume.
Santangelo, N., Horstman, H., and Horstman-Moretti, E.: 1973, *Solar Phys.* **29**, 143.
Tomblin, F. F.: 1972, *Astrophys. J.* **171**, 377.